Bioactive Materials 38 (2024) 499–511

Contents lists available at ScienceDirect

Bioactive Materials

journal homepage: www.keaipublishing.com/en/journals/bioactive-materials

Vascular units as advanced living materials for bottom-up engineering of perfusable 3D microvascular networks

I.D. Orge [a,c], H. Nogueira Pinto [a], M.A. Silva [a,b], S.J. Bidarra [a,b], S.A. Ferreira [a], I. Calejo [a], R. Masereeuw [d], S.M. Mihăilă [d], C.C. Barrias [a,b,c,*]

[a] i3S – Instituto de Investigação e Inovação em Saúde, Universidade do Porto, Porto, Portugal
[b] INEB-Instituto de Engenharia Biomédica, Universidade do Porto, Porto, Portugal
[c] ICBAS-Instituto de Ciências Biomédicas Abel Salazar, Universidade do Porto, Porto, Portugal
[d] Division of Pharmacology, Utrecht Institute for Pharmaceutical Sciences, Utrecht University, Utrecht, the Netherlands

ARTICLE INFO

Keywords:
Engineered tissue
Organ-on-chip
Microtissue
Spheroid
endothelial colony-forming cells

ABSTRACT

The timely establishment of functional neo-vasculature is pivotal for successful tissue development and regeneration, remaining a central challenge in tissue engineering. In this study, we present a novel (micro)vascularization strategy that explores the use of specialized "vascular units" (VUs) as building blocks to initiate blood vessel formation and create perfusable, stroma-embedded 3D microvascular networks from the bottom-up. We demonstrate that VUs composed of endothelial progenitor cells and organ-specific fibroblasts exhibit high angiogenic potential when embedded in fibrin hydrogels. This leads to the formation of VUs-derived capillaries, which fuse with adjacent capillaries to form stable microvascular beds within a supportive, extracellular matrix-rich fibroblastic microenvironment. Using a custom-designed biomimetic fibrin-based vessel-on-chip (VoC), we show that VUs-derived capillaries can inosculate with endothelialized microfluidic channels in the VoC and become perfused. Moreover, VUs can establish capillary bridges between channels, extending the microvascular network throughout the entire device. When VUs and intestinal organoids (IOs) are combined within the VoC, the VUs-derived capillaries and the intestinal fibroblasts progressively reach and envelop the IOs. This promotes the formation of a supportive vascularized stroma around multiple IOs in a single device. These findings underscore the remarkable potential of VUs as building blocks for engineering microvascular networks, with versatile applications spanning from regenerative medicine to advanced *in vitro* models.

1. Introduction

The presence of a well-developed vascular network in bioengineered tissues and organs is crucial for their functionality and applicability in therapeutic regeneration and disease modelling. The vascular system is among the first systems to develop during embryogenesis, as it is key to supporting and nourishing other tissues and organs [1,2]. It presents an intricate branching pattern, with larger diameter vessels giving rise to intricate networks of progressively smaller ones, ensuring that nearly every cell in the human body is located within a distance of only a few hundreds of micrometers from a capillary [3]. Capillaries, the most prevalent vessels, are lined by a single layer of endothelial cells (EC), supported by basement membrane (BM) and pericytes, and their diameter typically ranges from 5 to 10 μm [4]. Capillary networks play a central role in tissue homeostasis, enabling the exchange of oxygen, carbon dioxide, nutrients, and metabolites between the bloodstream and the adjacent tissues. Therefore, establishing a functional (micro)vasculature down to the capillary scale in engineered tissues and organs is key to preserving cell viability and function, remaining a central challenge in regenerative medicine strategies.

The field of 3D bioprinting has witnessed significant progress in the ability to generate tubular structures with higher resolution and increased complexity, opening up new possibilities for fabricating blood vessel-like networks with precise architectures [5,6]. However, printing

Peer review under responsibility of KeAi Communications Co., Ltd.
* Corresponding author. i3S – Instituto de Investigação e Inovação em Saúde, Universidade do Porto, Porto, Portugal.
E-mail addresses: iasmim.orge@i3s.up.pt (I.D. Orge), henriquenpinto@gmail.com (H. Nogueira Pinto), martas@i3s.up.pt (M.A. Silva), sbidarra@ineb.up.pt (S.J. Bidarra), silvia.ferreira@i3s.up.pt (S.A. Ferreira), icalejo@i3s.up.pt (I. Calejo), R.Masereeuw@uu.nl (R. Masereeuw), s.mihaila@uu.nl (S.M. Mihăilă), ccbarrias@i3s.up.pt (C.C. Barrias).

https://doi.org/10.1016/j.bioactmat.2024.05.021
Received 1 May 2024; Accepted 8 May 2024
Available online 15 May 2024

hollow structures at the capillary scale still represents a major challenge. Furthermore, in native tissues, the development of capillary beds follows a stochastic process, devoid of precise geometrical patterns, where the local microenvironment dynamically shapes ECs assembly into capillary networks that meet the unique metabolic demands of each organ [7]. This highlights the complexity of microvascularization processes, suggesting that engineered capillary networks should ideally develop *in situ*, tailored to the specific context.

Harnessing living (micro)materials as building blocks for generating microvascular networks from the bottom-up offers an exciting approach toward this goal. In our prior studies we reported the ability to create capillary-like structures from vascularized microtissues composed of EC and dermal fibroblasts or mesenchymal stem cells [8–10]. Expanding upon our previous findings, here we explored the use of vascularized microtissues (hereafter designated as Vascular Units, VUs) as versatile tools for generating perfusable stroma-embedded microvascular networks. We selected the small intestine as the target organ, as there is a pressing need for tissue engineering solutions in intestinal wound healing and a well-vascularized stroma is essential to support epithelial regeneration [11]. Notably, considering that minimally invasive laparoscopic procedures currently set the standard in clinical interventions for intestinal wounds, the micro-scale size of VUs positions them as an ideal system for this type of procedure [12].

We started by optimizing the biofabrication of VUs composed of human endothelial progenitors (endothelial colony-forming cells, ECFC) and organ-specific intestinal fibroblasts (hIF). ECFC presents high expansion potential and recognized ability to form de novo blood vessels *in vivo*, which makes them an ideal source for microvascular engineering [13]. On the other hand, fibroblasts act as supportive stromal cells, namely by producing extracellular matrix (ECM), which plays a key role in stabilizing the nascent microvessels, and may also act as pericytes [14]. The VUs were integrated in fibrin hydrogels to promote angiogenic sprouting and formation of lumenized endothelial networks. To better characterize their microvascularization potential, VUs were incorporated in a customized fibrin-based biomimetic vessel-on-chip (VoC) featuring endothelialized microfluidic channels with angiogenic sprouting potential. This allowed us to demonstrate the ability of VUs to inosculate (i.e., connect and integrate) with larger-diameter vessel-like microchannels and become perfused; to establish capillary bridges between channels; and to extend a stromal-embedded microvascular network throughout the entire device.

Finally, as a preliminary proof-of-concept, we demonstrated the applicability of VUs to promote the formation of a vascularized stroma in organoid cultures within the VoC. While organoids mimic important characteristics of native epitheliums, they still present limitations in achieving truly *in vivo*-like functionality. In particular, the absence of an external vascular supply and adequate stromal support may hinder proper growth, shorten lifespan, and impair functionality by preventing adequate differentiation and maturation [15]. Therefore, the development of effective strategies for organoid vascularization remains a challenge in the field [7,16]. Here we show that the combination of VUs with IOs within the VOC offers a promising approach to promote the formation of a vascularized stroma around multiple organoids in one single microfluidic device. The formation of an ECM-rich fibroblastic stroma is per se relevant, as highly regenerative organs, like the intestine, strongly rely on fibroblast activity to maintain the stem cell niche [17].

Collectively, by providing versatile building blocks for *in situ* generation of perfusable microvascular beds embedded in stromal tissue, VUs offer a valuable tool for tissue engineering, with far-reaching implications in the fields of regenerative medicine, 3D *in vitro* models, and organ-on-chip (OoC).

2. Materials and methods

2.1. Vascular units (VUs)

2.1.1. Cells sources and maintenance

Human umbilical cord blood was obtained from healthy donors following a protocol approved by the Ethics Committee of CHUSJ (Centro Hospitalar Universitário de São João, Porto, Portugal). Endothelial colony forming cells (ECFC) were isolated from umbilical cord blood as previously described [18–20]. All blood donors were kept anonymous, so the need for written consent was waived. Cells were maintained in ECFC growth medium composed of MCDB-131 basal medium (BM) supplemented with 5 % v/v fetal bovine serum (FBS), 1 % v/v of penicillin-streptomycin (Pen/Strep), 2 mM L-glutamine, 1 μg/mL ascorbic acid, 0.2 μg/mL hydrocortisone, 2 ng/mL VEGF, 20 ng/mL IGF-1R, 10 ng/mL FGF, and 5 ng/mL EGF. Cells were used at passages 5 to 8. Primary human intestinal fibroblasts (hIF) were acquired from Innoprot©. Cells were maintained on DMEM/F12 medium supplemented with 10 % v/v FBS and 1 % v/v Pen/Strep. Cells were used at passages 5 to 10. Both cell types were routinely cultured at 37 °C under a 5 % v/v CO_2 humidified atmosphere and passage upon reaching ~80 % confluence. The culture medium was changed every 2 days for ECFC and every 3 days for hIF.

2.1.2. Generation of vascular units (VUs)

VUs were generated using MicroTissues® 3D Petri Dish® technology as previously described [9]. Briefly, agarose-based micro-molds (2 % w/v agarose in 0.9 % w/v NaCl) were prepared using commercial templates (9x9 or 16x16 microwell arrays), placed in 12-well tissue culture plates and equilibrated with basal MCDB-131 medium overnight. ECFC and hIF were trypsinized and resuspended in their respective media. For 9x9 arrays, cells were seeded at a total density of 12,000 cells/spheroid in 200 μL of EC growth medium at hIF:ECFC ratios of 1:1 (6000 hiF + 6000 ECFC) and 5:1 (10,000 hiF + 2000 ECFC). For 16x16 arrays, cells were seeded at a total density of 6000 cells/spheroid in 200 μL of EC growth medium at hIF:ECFC ratio of 1:1 (3000 hiF + 3000 ECFC). Cells were allowed to settle for 30 min at room temperature (RT), and then additional medium was added to the wells. The medium was changed every 2 days. VUs were collected for analysis after 1, 5, and 7 days of culture. The metabolic activity of VUs was assessed with CellTiter-Glo® 3D Cell Viability Assay (ProMega) according to the manufacturer's instructions. Briefly, VUs were transferred from the mold to a white opaque-walled 96-well plate in 100 μL of growth medium (4 VUs per well) and 100 μL of CellTiter-Glo® 3D Reagent was added to each well. The plate was shaken in the microplate reader (Synergy MX, BioTek) for 5 min and incubated at room temperature for 25 min. After incubation, luminescence was measured using a microplate reader (Synergy Mx, BioTek, integration time of 1 s, sensitivity of 135, top probe vertical offset of 1 mm).

2.1.3. Hydrogel embedding

Fibrin hydrogels were optimized according to previously published protocols [9,10]. A fibrinogen solution (Sigma) was prepared in NaCl 0.9 % w/w mixed with aprotinin (Sigma) and diluted in EC growth medium to final concentrations of 2 mg/mL and 25 μ/mL, respectively. For VUs embedding, these were added to the fibrinogen solution, mixed with thrombin (2 U/mL in PBS) at 4:5 v/v ratio and left for 30 min at 37 °C for crosslinking.

2.1.4. Gene expression analysis

RNA was extracted from VUs using the Quick-RNA MiniPrep (Zymo Research), following the manufacturer instructions. Subsequently, 500 ng of total RNA was reversed transcribed to single stranded cDNA using the Takara cDNA synthesis kit. Quantitative Real-Time PCR (qRT-PCR) was carried out using source RNA from 3 biological replicates (i.e., 3 individual experiments) for the target genes *Col1a1*, *PECAM1*, *CDH5*,

LMNA, KDR, FLT1 and for endogenous control *GAPDH* using as probe sets Hs. PT.58.1551779, Hs. PT.58.19487865, Hs. PT.58.4732035, Hs. PT.58.27794, Hs. PT.58.3285240, Hs. PT.58.40906831 and Hs. PT.51.1940505 (Applied Biosystems and Integrated DNA Technologies), respectively. Samples were run in triplicates in the ABI Prism 7000 Sequence Detection System under the following conditions: 95 °C for 20 s, followed by 40 cycles at 95 °C for 3 s and 60 °C for 30 s. The expression value for each target gene was normalized to GAPDH value for all the samples.

2.1.5. Immunohistochemistry analysis of VUs

VUs were fixed inside the agarose micromolds with 4 % w/v PFA (30 min, RT). The molds were then sealed with 200 μL of molten HistoGel™ (ThermoFisher) and processed in an automatic rotational tissue processor (STP-120-1, MICROTOM). Samples were paraffin-embedded in an EC-350 embedding center and sectioned into 6 μm sections. Afterwards, sections were deparaffinized in xylene and rehydrated in sequentially decreasing ethanol concentrations. Antigen retrieval was performed with TE buffer (10 mM Tris, 1 mM EDTA, pH 9) or sodium citrate (10 mM, pH 6), at 95 °C for 30 min. Sections were permeabilized in 0.25 % v/v Triton X-100 (Sigma) for 10 min, blocked with 5 % v/v FBS 1.5 % w/v BSA in PBS for 1 h at room temperature and incubated overnight with the following primary antibodies diluted in blocking solution: mouse anti-CD31 (Dako, 1:100); rabbit anti-fibronectin (FN, Sigma, 1:200); rabbit anti-laminin (LAM, Sigma, 1:100); mouse anti-collagen type IV (COL IV, Dako, 1:100); rabbit anti-collagen type I (COL I, Rockland, 1:100). Sections were then washed with PBS and incubated with the corresponding fluorochrome-conjugated secondary antibodies (Alexa-Invitrogen, 1:500) and 4′,6-diamidino-2-phenylindole (DAPI, 1:1000) for 1 h at RT. Samples were washed and mounted with VectaShield (Vector).

Hydrogel-embedded VUs were analyzed as whole-mounted samples at pre-defined time points (days 1, 3, 5 or/and 7, depending on the experiment). Samples were washed with PBS and fixed with 4 % w/v PFA (30 min, RT). Then, gels were permeabilized with 0.25 % v/v Triton X-100 for 20 min, blocked with 5 % v/v BSA in PBS for 1 h at room temperature and incubated overnight with Alexa Fluor 647 Phalloidin (Invitrogen, 1:1000), Ulex Europaeus Agglutinin I Rhodamine (UEA I) (Vectors, 1:400) and the following primary antibodies diluted in 1 % w/v BSA: mouse anti-human CD31 (Dako, 1:100); rabbit anti-human fibronectin (FN, Sigma, 1:200); rabbit anti-laminin (Sigma, 1:100); mouse anti-human vimentin (VIM, Santa Cruz, 1:100) and mouse anti-human alpha smooth muscle actin (α-SMA, Abcam, 1:200). Samples were washed with 0.05 % v/v Tween-20 and incubated with the corresponding fluorochrome-conjugated secondary antibodies (Alexa 488 anti-mouse, Alexa 488 anti-rabbit, Alexa 594 anti-mouse and/or Alexa 594 anti-rabbit, Invitrogen, 1:500) and DAPI (1:1000) for 4 h at RT.

Images were acquired using a Leica TCS SP5 AOBS spectral confocal microscope (Leica Microsystems, Germany) or in a high-content screening system equipped with a fully automated widefield/confocal fluorescence microscope (Opera Phenix Plus, Revvity).

2.2. Microfluidic device

2.2.1. Fabrication of the microfluidic chamber and culture-on-chip

The polylactic acid (PLA) core of the chamber was 3D printed using the Fused Deposition Modeling method and the final design was optimized based on a previously reported set-up [21–23] (Fig. S1A, Supporting Information). Briefly, melted PLA layers of 100 μm height were deposited in precise locations in a layer-by-layer approach to create the object. Then, two fluid dispensing tips of 18 G (Nordson EFD) were inserted into both lateral holes on the sides of the chamber and fixed with epoxy glue. The chamber was then bonded to a glass slide with the same glue and left to dry overnight at room temperature. Pipette tips were used as reservoirs by inserting them into the chamber inlets. For the formation of a perfusable channel in the central reservoir of the microfluidic chamber, an acupuncture needle (300 μm diameter) was inserted inside the tip inlet and the reservoir was filled with the fibrinogen-thrombin solution for *in situ* fibrin formation. For studies with VUs, these were added to the hydrogel-precursor solution before loading into the chamber (Fig. S1, Supporting Information). After crosslinking, the needle was carefully removed, and the resulting hollow channel was coated with a fibronectin-collagen solution [24]. In some experiments, we used an alternative VoC setup, incorporating two perfusable hollow channels instead of only one (Fig. S1, Supporting Information). For endothelization, ECFC and hIF (10:1 ratio) suspended in EC growth medium were loaded into the channel at C1 = 1×10^5, C2 = 5×10^5 or C3 = 10×10^5 cells per channel. After 2 h, medium was added to the central well and the tip reservoirs. The chips were cultured under static conditions for the first 24 h after channel endothelization and then transferred to a rocking tilting platform (minimum speed of 4 rpm), which was maintained at 37 °C under a 5 % v/v CO_2 humidified atmosphere for 1–2 weeks. Medium (EGM-2MV) inside the channels and central chamber was refreshed daily.

2.2.2. Perfusion assays

The basal fluorescence level of the system was acquired and then fluorescent tracers were added to the microfluidic channels: either soluble dextran (50 μL, 1:100 in PBS, 70 kDa FITC-Dextran, Sigma) or fluorescent microbeads (2 μm size, 1:1000 in PBS, FluoSpheres™ carboxylate-modified microspheres, ThermoFisher Scientific). ECFC were labeled with Agglutinin I Rhodamine (UEA I) (Vectors, 1:400) for analysis of FITC-Dextran or with mouse anti-human CD31 (Dako, 1:100) for analysis of fluorescent beads. Both fluorescent tracers were added to the inlet of the device which was tilted to induce gravity-driven flow to the outlet. After 5 min of perfusion, the device was imaged in a Leica TCS SP5 AOBS spectral confocal microscope (Leica Microsystems, Germany) or in a high-content screening system equipped with a fully automated widefield/confocal fluorescence microscope (Opera Phenix Plus, Revvity).

2.2.3. Gene expression and immunofluorescence analysis

For gene expression analyses, the VUs loaded fibrin hydrogel were removed from the central chamber with a spoon and incubated with 3 mg/mL nattokinase solution for 20 min at 37 °C for fibrin degradation and VUs recovery. Subsequently, RNA extraction, cDNA production and qRT-PCR proceeded as described above for the target genes *PECAM1*, *CDH5*, *LMNA*, *FLT1*(Hs.PT.58.40906831) and *MMP2* (Hs. PT.58.39114006) (Applied Biosystems and Integrated DNA Technologies). Samples were run in triplicates in the ABI Prism 7000 Sequence Detection System under the following conditions: 95 °C for 20 s, followed by 40 cycles at 95 °C for 3 s and 60 °C for 30 s. The expression value for each target gene was normalized to GAPDH value for all the samples.

For immunofluorescence analysis, the whole 3D construct was processed *in situ* as described above for hydrogel-embedded samples and imaged using a Leica TCS SP5 AOBS spectral confocal microscope (Leica Microsystems, Germany) and the Opera Phenix® Plus High-Content Screening System (Revvity).

2.3. Organoid culture

2.3.1. Crypt isolation and culture of intestinal organoids (IOs)

Surplus C57bl/6 mice were used for the crypt isolation procedure using a previously published protocol [25,26]. Briefly, a distal segment of the intestine was harvested, separated from the cecum, and flushed with cold PBS to remove stool. Then, the intestine was opened longitudinally with a scissor and internal mucosa was scraped to remove villi. The tissue was washed in cold PBS, chopped with a surgical blade into 2–4 cm pieces and incubated in 500 mM EDTA (Sigma) for 1 h on ice. After incubation, the tissue was resuspended in cold PBS and hand-shaken (2–3 cycles per second) to dissociate epithelium from the

basement membrane and further remove the villi from the crypts. The suspension was transferred to a 70 μm filter and centrifuged for 10 min at 150 g at 4 °C. The pellet was resuspended in PBS and crypts counted in 10 μL drop using a Petri dish. A solution of 12,500 crypts/mL of Matrigel (Corning) was prepared and 40 μL domes were seeded in 24 well plates. After 30 min at 37 °C, Intestinal Organoids Medium was added to the wells (Advanced DMEM/F12 with Glutamax and HEPES (Gibco), 1x B27 (Gibco), 1x N2 (Gibco), 1.25 mM *N*-acetylcysteine (20 mg/mL in H_2O, Sigma), 10 % v/v *R*-spondin (conditioned medium), 10 % v/v Noggin (conditioned medium), 100 μg/mL v/v Primocin (InvivoGen), and 50 ng/mL EGF (PeproTech). Medium was changed every 2 days and IOs were passaged every week. To passage or collect IOs for other experiments, 1 mL of ice-cold PBS was added to each well and domes were mechanically dissociated by pipetting up and down vigorously. The suspension was collected to a 15 mL tube and centrifuged for 10 min at 1200 rpm, 4 °C. Supernatant was carefully discarded, and the pellet was resuspended in the appropriate volume of IO medium. Passage ratio was usually 1-to-3 domes.

For hydrogel-embedding, IOs alone or combined with VUs were added to Matrigel or to fibrin-based hydrogels. Three types of fibrin-based hydrogels were tested: 1) Fib (non-supplemented fibrin: 1.5 mg/mL fibrinogen with 25 μg/mL aprotinin), 2) Fib-LEC (fibrin supplemented with 2 mg/mL of LEC, laminin-entactin complex, Corning), and Fib-MG (fibrin supplemented with 10 % v/v Matrigel™). To trigger polymerization of fibrin hydrogels, thrombin (2 U/mL) was added at 4:5 v/v ratio.

2.3.2. Oscillation rheometry analysis

The rheological properties of the hydrogels were analyzed by oscillatory shear rheometry (Kinexus Pro rheometer, Malvern) using a cone-on-plate (0.5°/40 mm) geometry. Each gel-precursor solution was prepared and immediately poured on the plate for analysis. A solvent trap filled with water was used to minimize sample drying. The evolution of the shear moduli, G′ (storage, elastic component) and G″ (loss, viscous component) was recorded at 37 °C as a function of time for 30 min. A frequency of 0.5 Hz and a strain of 1 % were applied to maintain the linear viscoelastic regime. Three replicates were used for each condition.

2.3.3. Immunofluorescence analysis

Samples were processed and imaged as described above but using the following additional antibodies: mouse anti-human β-catenin (β-CAT, BD Biosciences, 1:100); rabbit anti-E-cadherin (E-CAD, Cell signaling, 1:100); rabbit anti-Ki-67 (Abcam, 1:100), rabbit anti-lysozyme (Invitrogen, 1:100).

2.4. Image analysis

Images were analyzed using ImageJ 1.50i software and Harmony high-content analysis software 4.8 was used for 3D images reconstructions generation. An image analysis tool developed by Ivanov et al. [27] for Fiji/ImageJ software was adapted to analyze VUs morphology within the molds, using brightfield images. The VUs area was automatically determined, and average diameter was calculated assuming a perfect circle. Sprouting from VUs embedded in fibrin was quantified and morphologically evaluated using the image analysis tools "CLIJ" [28] and "Angiogenesis" [29], for FIJI/ImageJ software (Fig. S2B, Supporting Information). Briefly, two Gaussian blur filters with different kernels were applied to a CD31 staining image with "Difference of Gaussians" function of CLIJ, and the two resulting images subtracted to each other, removing background and isolating the sprouts in a new image which was then merged with the corresponding DNA staining image. Thereafter, "Sprout Morphology" function of "Angiogenesis" plug-in was able to detect spheroids, sprouts that were originated from those spheroids, and cell nuclei in each sprout. Different parameters for each step were screened and selected based on sprout and VUs detection efficiency and accuracy.

Sprouting from both cropped sides of the endothelized channel of the microfluidic device was quantified using the image analysis tool "Angiogenesis analyzer" for FIJI/ImageJ software [30]. Briefly, a Median filter followed by a Gaussian blur filter was applied to the cropped right and left sides images acquired from a randomized central area of the channel. Total sprouts number was calculated using the sum of segments and branches detected by the tool.

2.5. Statistical analysis

All the statistical analyses were performed using GraphPad Prism 8.3.0 software. For the data represented in the graphs depicted in Figs. 1 and 2, 2-way ANOVA and Bonferroni's multiple comparisons test were used for the analysis. D'Agostino & Pearson normality test was applied for the graphs of Fig. 3E and H and the data was analyzed using one-way ANOVA Tukey's multiple comparisons test. All data were analyzed using the non-parametric Mann-Whitney test using a 99 % confidence interval and statistically significant differences are marked with * ($p < 0.05$), ** ($p < 0.01$), *** ($p < 0.001$), or **** ($p < 0.0001$).

3. Results

3.1. VUs generate lumenized microvascular networks inside fibrin

VUs composed by hIF and ECFC combined at cell ratios of 5:1 (10,000 hIF + 2000 ECFC) and 1:1 (6000 hIF + 6000 ECFC) were produced and cultured for up to 1 week in non-adhesive agarose microwells (Fig. 1A). The overall metabolic activity (Fig. 1B) significantly decreased after 5 and 7 days of culture, independently of the cell ratios. This in line with our prior research using dermal fibroblasts or mesenchymal stem cells as supportive stromal cells [9,10] and is likely associated with the gradual transition from a more active to a nearly quiescent phenotype during spheroid culture. In turn, the cell ratio influenced the VUs size, the ECFC organization, and the global expression of endothelial markers and ECM proteins. VUs with higher proportion of hIF (5:1) presented a smaller size than the 1:1 VUs (Fig. 1B), possibly due to the tissue-contraction potential of fibroblasts and their ability to produce large amounts of ECM (Fig. 1C–S3 and S4, Supporting Information), which acts as a "glue" contributing to the higher densification and contraction of VUs. Along the time, in both ratios, some of the ECFC ($CD31^+$) segregated into the VUs' surface, while others formed clusters at the core, which developed into aligned endothelial structures in the 5:1 VUs (Fig. 1C). In VUs with lower proportion of hIF (1:1), some ECFC were gradually excluded from the VUs, as shown by the presence of released $CD31^+$ cell clusters (Fig. 1C). This was accompanied by a decrease in the number of $CD31^+$ cells at the VUs' outer layer from day 1 to day 7 (Fig. 1D and S4, Supporting Information). This is possibly due to insufficient stromal support, as previously observed [9,10]. After 7 days, abundant amounts of ECM components (collagen type I and IV, laminin) were present in VUs, forming a well-defined layer on the surface and exhibiting a more random organization in the interior (Fig. 1C). The mRNA expression levels of endothelial and ECM markers (Fig. 1E) aligned with the immunofluorescence results. At day 1, the 1:1 VUs (with 3 times more ECFC than 1:5 VUs) showed higher expression of the endothelial markers *PECAM1* (CD31), *CDH5* (VE-cadherin), *KDR* (VEGF receptor 1), *FLT1* (VEGF receptor 1 and the basement membrane (BM) marker *LMNA*. From day 1 to day 7, the expression levels in 1:1 VUs decreased significantly, probably reflecting the loss of ECFC along the culture. In contrast, the expression of *PECAM, KDR*, and *FLT1* in 5:1 VUs increased from day 1–7, which may reflect the higher degree of ECFC organization and formation of primitive vessel-like structures at the VUs core. In both ratios, there was an increased expression of *Col1a1* from day 1 to day 7, which likely reflects sustained ECM production and accumulation inside VUs.

After characterization, VUs were collected after 1 day of spheroid culture, when they showed higher metabolic activity and higher ECFC

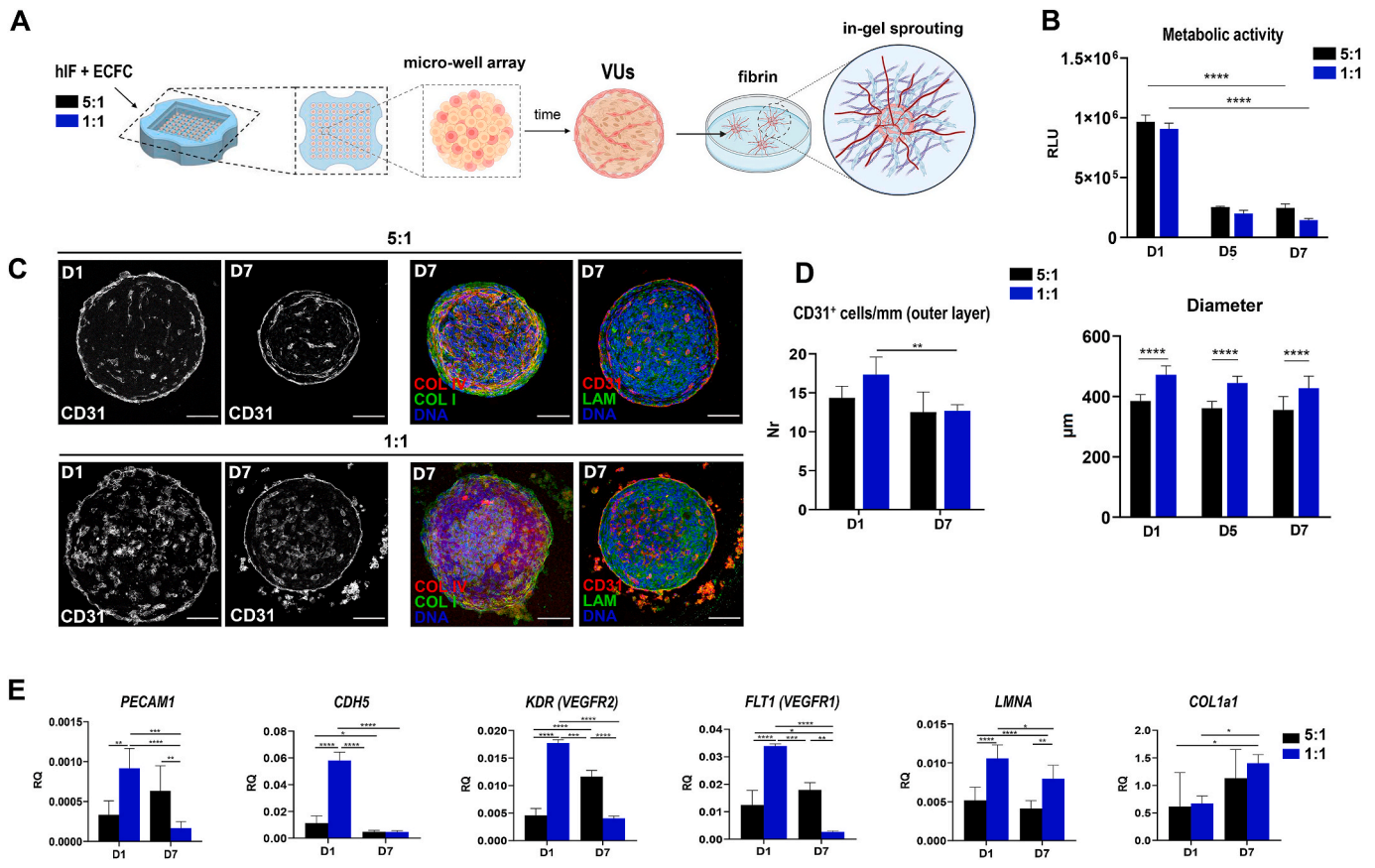

Fig. 1. Endothelial cells segregate and organize at the outer layer and at the core of VUs. A) Graphical representation of VUs production using agarose microwell-molds and subsequent embedding in fibrin hydrogel. Created with BioRender.com. **B)** Metabolic activity and diameter of VUs with different hIF-to-ECFC ratios (5:1 and 1:1) after 1–7 days of culture (n = 3 independent experiments, 2 technical replicates each). **C)** Immunofluorescence images showing the organization of ECFC ($CD31^+$ cells) in VUs (5:1 and 1:1) after 1 and 7 days of culture and ECM production at day 7 (scale bars: 75 μm). **D)** Quantification of $CD31^+$ cells on the outer layer of VUs (5:1 and 1:1) at day 1 and 7. **E)** mRNA expression (qPCR analysis) of *PECAM1* (encodes for CD31), *CDH5* (encodes for VE-cadherin), *KDR* (encodes for VEGFR2), *FLT1* (encodes for VEGFR1), *LMNA* (encodes for laminin) and *Col1a1* (encodes for collagen type I). In all graphs, statistically significant differences are marked with * ($p < 0.05$), ** ($p < 0.01$), *** ($p < 0.001$), or **** ($p < 0.0001$).

amount, embedded in fibrin and cultured for an additional week. The hydrogel provided a favorable 3D environment for angiogenic sprouting, leading to the rapid formation of multiple VUs-derived capillary-like structures. As the culture progressed over 7 days, the number of sprouts decreased, as they merged into larger diameter structures, and their length increased (Fig. 2A and B). As the 1:1 VUs showed enhanced levels of active sprouting (shortly after embedding) and lengthier sprouts (after 7 days of culture) they were selected for the subsequent studies. The VUs-derived capillaries were surrounded by a laminin-rich BM-like layer and presented distinct lumens (Fig. 2C). The hIF (VIM^+ cells) were also observed to migrate out of the VUs and invade the surrounding hydrogel, contributing to the production of ECM in the external space and to the stabilization of the formed microvascular structures (Fig. 2D). Notably, α-SMA^+ cells were found close to vWF^+ microvessels, suggesting that some of the hIF committed to pericyte-like mural cells (Fig. S5, Supporting Information). Remarkably, capillaries originating from neighboring VUs showed the ability to grow towards each other (Fig. 2E–i) and merge (Fig. 2E–ii). This inosculation potential, along with the ability of VUs to fuse with other VUs at the core level (Fig. 2E–iii), ultimately led to the formation of extensive microvascular networks (Fig. 2E–iv) with elongated capillaries spanning up to 5 mm in length after 1 week of culture. These structures remain stable for at least 2 weeks in culture (data not shown). Collectively, these findings showcase the suitability of VUs as building blocks for the bottom-up generation of robust microvascular 3D networks.

3.2. Establishment and perfusion of a biomimetic fibrin-based VoC

To further characterize the VUs-derived capillaries and microvascular networks, we designed a customized microfluidic device (vessel-on-chip, VoC), incorporating a hollow channel within the fibrin hydrogel, all contained within a perfusable PLA holder (Fig. 3A). The hydrogel precursor solution was introduced into the central chamber of VoC over a needle that was removed after polymerization, forming a hollow channel (with an average diameter of ~300 μm). This arteriole-like microfluidic channel was perfused with a blue dye using a peristaltic pump, which validated its flexibility, structural integrity, and ability to accommodate flow rates within the range of 1–10 μL/min without bursting (Supporting Information, videos). To ensure successful endothelialization, the hollow channel was pre-coated with ECM proteins prior to cell seeding (Fig. 3B). Notably, the entire structure, i.e., the hydrogel matrix with the embedded channel, with or without cells, could be readily retrieved from the PLA chamber using a spatula, without compromising its structural integrity (Fig. 3C i-v). Additionally, the fibrin hydrogel could be enzymatically degraded under mild conditions yielding a self-standing endothelialized vessel-like structure (Fig. 3C vi-vii and Fig. S6, Supporting Information), which greatly facilitated downstream analysis.

We tested various cell densities: C1 (1×10^5 cells), C2 (5×10^5 cells), and C3 (10×10^5 cells), to promote the endothelialization of the hollow channel (Fig. S7, Supporting information). Our findings revealed that the cell density had a significant impact on the performance and

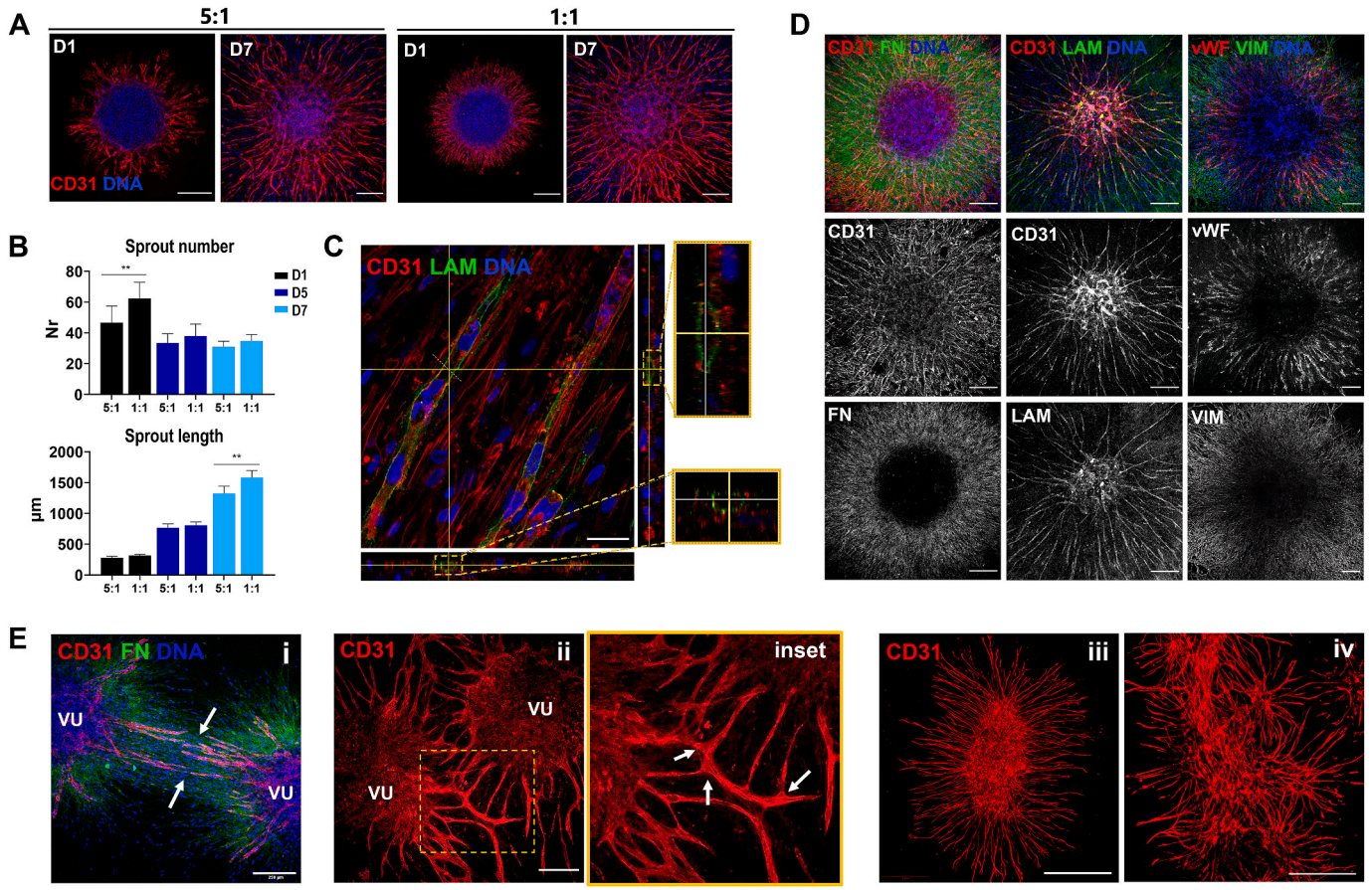

Fig. 2. VUs form extensive microvascular 3D networks when embedded in fibrin. A) Immunofluorescence images showing angiogenic sprouting from VUs in fibrin (5:1 and 1:1) at days 1 and 7 post-embedding (red: CD31, blue: nuclei, scale bars: 250 µm). **B)** Average number and length of VUs-derived capillaries (5:1 and 1:1) at days 1, 5, and 7 post-embedding. **C)** Higher magnification image showing a laminin-rich BM-like layer enveloping the VUs-derived capillaries (green: laminin, red: CD31, blue: DNA, scale bar: 50 µm) and the presence of lumens (orthogonal views). **D)** Immunofluorescence images showing VUs-derived capillaries ($CD31^+$ cells), outward migration of hIF (VIM^+ cells), and deposition of ECM proteins (LAM and FN) in the fibrin hydrogel surrounding 1:1 VUs after 7 days in culture (scale bars: 250 µm). **E)** Immunofluorescence images showing: i) the ability of VUs-derived capillaries (1:1) to grow towards each other and ii) inosculate; and iii) the ability of VUs to fuse with other VUs and iv) form extensive microvascular networks (red: CD31, green: FN, blue: DNA). Scale bars: 250 µm (i), 200 µm (ii); 1 mm (iii-iv). In all graphs, statistically significant differences are marked with * ($p < 0.05$), ** ($p < 0.01$), *** ($p < 0.001$), or **** ($p < 0.0001$).

organization of the resulting endothelial layer. While the lower cell-seeding density (C1) resulted in a stable endothelial monolayer (Fig. 3D and E), higher cell densities (C2, C3) led to the formation of a pro-angiogenic endothelium, from which lumenized endothelial sprouts emerged, extending into the hydrogel bulk (Fig. 3D and E). The hIF also migrated from the microchannel into the fibrin, contributing to the formation of stromal tissue within the hydrogel (Fig. 3F). Notably, the VoC channel-derived endothelial sprouts presented lumens up to 110 µm in diameter (Fig. 3G), with no significant differences between the C2 and C3 conditions in terms of sprout number and lumen diameter (Fig. 3E and H). Based on these findings, the intermediate condition (C2) was selected for further studies.

By perfusing the VoC microfluidic channel with FITC-Dextran (70 kDa), we provided evidence of "flow-through", with no apparent leakage, and of "flow-in" into the angiogenic sprouts (Fig. 3I). The VoC channel was also perfused with fluorescent microbeads (2 µm), which infiltrated the endothelial sprouts and accumulated at their open-ended branches, within the hydrogel matrix (Fig. 3J). For some of the studies with VUs (section 3.3), we used an alternative VoC setup, incorporating two perfusable hollow channels instead of only one. Overall, this customized VoC, composed only of fibrin and cells, provided an ideal biomimetic platform with no geometrical constraints to microvessel development, as envisaged.

3.3. The VUs-derived capillaries inosculate with VoC channels and form extensive microvessel networks

To further demonstrate the ability of VUs to generate extensive microvascular networks these were loaded into the VoC. The central chamber was filled with fibrin precursor solution and VUs were introduced close to (1-channel VoC) or between channels (2-channels VoC, Fig. 4A), prior to complete polymerization. As shown in Fig. 4B, the endothelial sprouts emerging from the VoC channel were unable to bridge the 2 mm gap between them and form connections with each other, even after 6 days of culture. In contrast, when VUs were also incorporated into the VoC, they rapidly formed capillaries that spanned the 2 channels, creating a microvascular 3D network. Fig. 4C depicts more detailed images of the system, showing VUs next to a VoC channel immediately after fibrin-embedding (day 0, 4C-i) and the formation of channel-derived and VUs-derived capillaries over time (day 5, 4C-ii). The length of the VUs-derived capillaries progressively increased, and the interactions between adjacent VUs contributed to the formation of a capillary network (Fig. 4C–ii and Fig. S8, Supporting Information). At day 5 there was already inosculation between capillaries from neighboring VUs (VU-VU, Fig. 4C–iii, dashed arrows), as well as between VUs-derived capillaries and the VoC channel (VU-VoC, Fig. 4C–iii, solid arrows). This facilitated the expansion of the microvascular network throughout the entire device. Fig. 4C–iii also shows the presence of

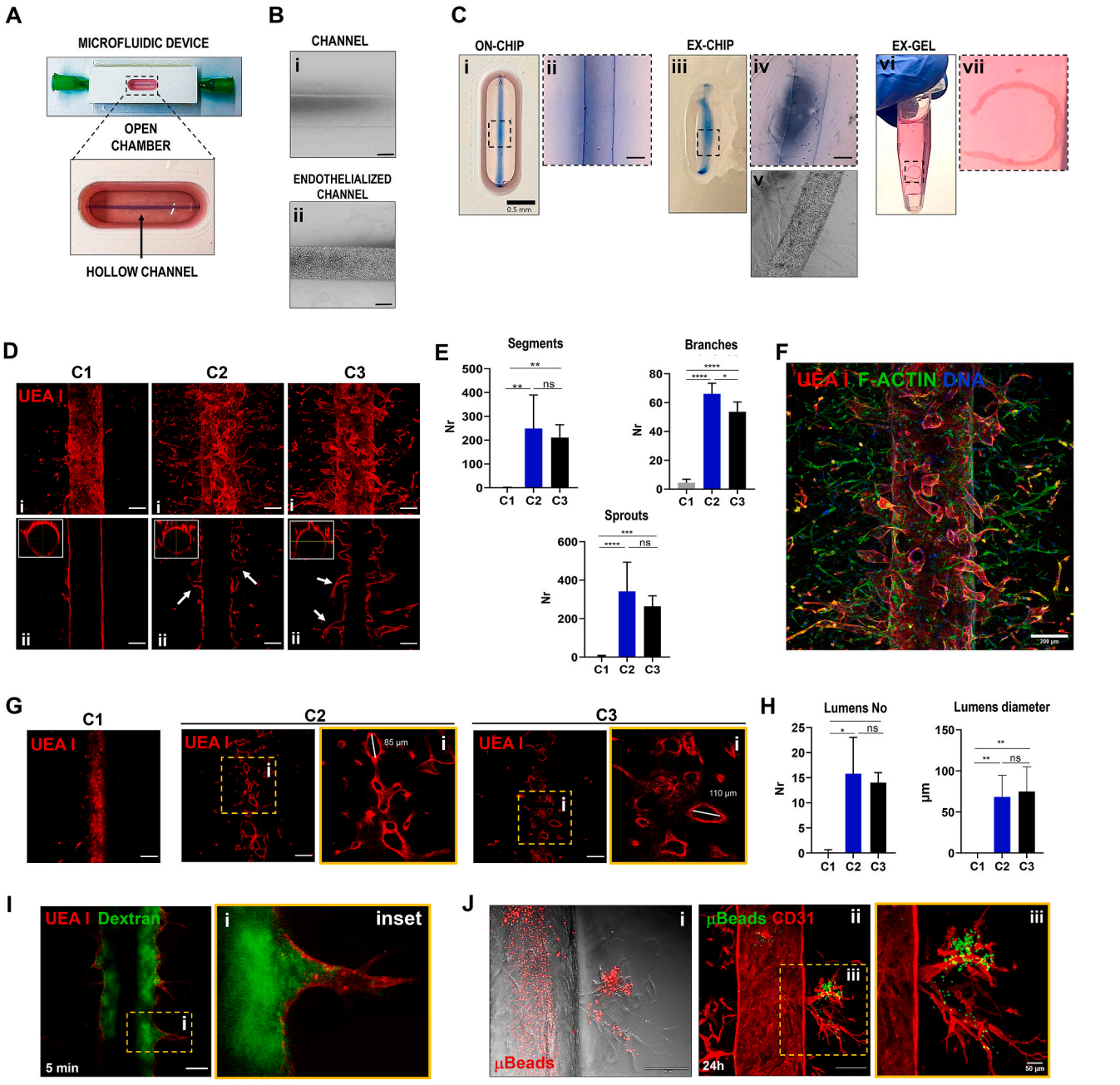

Fig. 3. The designed fibrin-based microfluidic device offers a biomimetic VoC. A) Top view of the microfluidic device showing the hollow channel perfused by blue dye**. B)** Phase-contrast images of the hollow channel (i) before and (ii) after endothelialization. Scale bars: 200 µm. **C)** i) image of the chamber perfused with blue dye (ii: magnification, scale bar: 200 µm); iii) image of the fibrin hydrogel removed from the chamber (magnifications showing iv-bare and v-endothelialized channels, scale bar: 200 µm); vi) image of endothelialized channel after enzymatic degradation of fibrin (vii: magnification). **D)** Representative immunofluorescence images of VoC loaded with different cell densities: 1×10^5 (C1), 5×10^5 (C2) or 10×10^5 (C3) cells (red, UEA I), (i-longitudinal and ii-transversal stacks showing the channel lumen and the lumenized endothelial sprouts (white arrows), scale bars: 200 µm. **E)** Quantification of the total number of segments, branches, and sprouts in representative areas of the VoC at different cell densities (n = 3 independent experiments, 2 channel areas per experiment). **F)** Immunofluorescence image showing the different cell types (ECFC and hIF, at C3) sprouting from the channel (red: UEA I, green: F-actin, blue: DNA, scale bar: 200 µm). **G)** Top stack view of the channel with different cell densities (C1, C2 and C3) showing the absence of endothelial sprouts in C1, and the presence of lumenized endothelial sprouts in C2 and C3 (red: UEA I, scale bars: 200 µm). **H)** Quantification of lumens number and diameter (n = 3 independent experiments, 2 channel areas per experiment). **I)** Immunofluorescence image showing a transversal stack of the VoC (red: UEA I) 5 min after perfusion with 70 kDa Dextran-FITC (green), scale bars: 200 µm (i: magnification). **J)** Perfusion of VoC with fluorescent microbeads for 5 min: i) phase-contrast composite image obtained immediately after perfusion (red: beads), ii) immunofluorescence image obtained 24 h after perfusion (red: CD31, green: beads), scale bars: 200 µm, iii) higher magnification image, scale bar: 50 µm. In all graphs, statistically significant differences are marked with * ($p < 0.05$), ** ($p < 0.01$), *** ($p < 0.001$), or **** ($p < 0.0001$).

fibroblasts ($CD31^-$ cells stained for f-actin, in green) that migrated from VUs, and formed a stromal network within the bulk fibrin hydrogel, around the VUs and the VoC channels. The stromal-embedded microvasculature became progressively more stable, transitioning from an 'active' pro-angiogenic state to a more mature vascular phenotype. This was corroborated by a decrease of the mRNA expression levels of endothelial markers (*PECAM1, CDH5, FLT1*), BM markers (*LMNA*), and matrix-remodeling markers (*MMP2*) decreased from day 1 to day 7

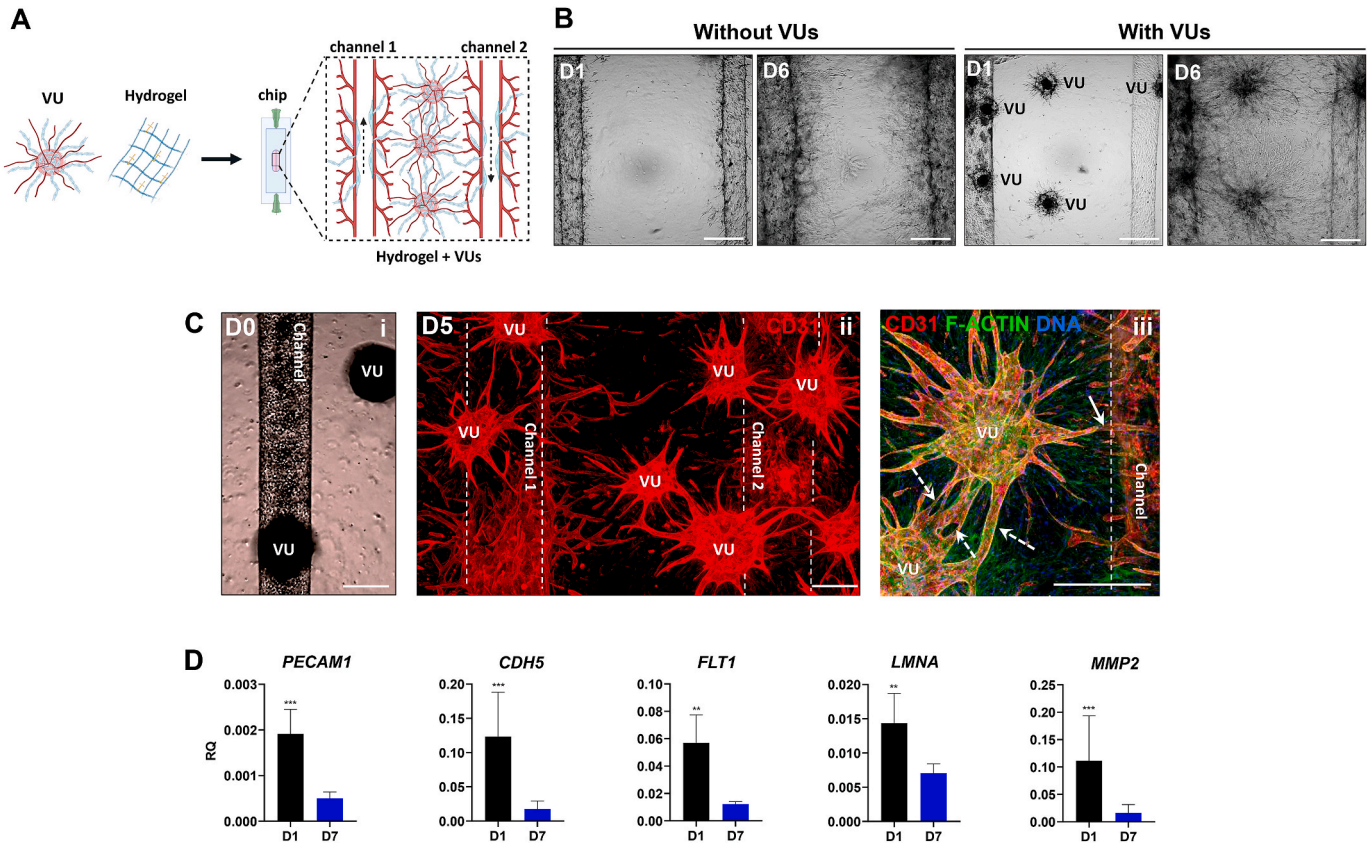

Fig. 4. VUs bridge the VoC channels and expand the microvascular network to the whole device. A) Graphical representation of the experimental setting of VUs assembly in the microfluidic device. Created with BioRender.com. **B)** Phase contrast images of the 2-channel VoC design without and with VUs at day 1 and 6 (scale bars: 500 μm). **C)** Phase-contrast (i) and fluorescent images (ii, iii) of VUs integrated in the chip at days 0 and 5. iii) higher magnification image (red: CD31, green: F-actin, blue: DNA, white dashed line: channel, scale bars: 200 μm) showing interconnections between VUs-derived capillaries (dashed arrows) and between VUs-derived capillaries and the channel (solid arrow). Fibroblasts correspond to the f-actin stained $CD31^-$ cells. **D)** mRNA expression of *PECAM1* (encodes for CD31), *CDH5* (encodes for VE-cadherin) and *FLT1* (encodes for VEGFR1), *LMNA* (encodes for laminin) and *MMP2* (encodes for matrix metalloproteinase 2) at days 1 and 7. In all graphs, statistically significant differences are marked with ** ($p < 0.01$) or *** ($p < 0.001$).

(Fig. 4D) [31,32].

3.4. The VUs-derived microvascular network is perfusable

Fig. 5A depicts the 3D volume visualization by Thermal Color LUT image of UEA-I^+ staining (ECFC cells), showcasing the close-distance positioning of a VU in relation to the VoC channel (Fig. 5A–i) and the interconnection between both structures (Fig. 5A–ii). While there was no significant difference in the average distances between VUs (VU-VU) and between VUs and the channel (VU-VoC) (Fig. 5B–i), the VU-VU interconnections were more frequent than the VU-VoC (Fig. 5B–ii). This was somewhat expected since there is only one channel but multiple VUs. Additionally, quantitative data demonstrated that the diameters of the VUs-derived microvessels had a homogenous size distribution, ranging from 10 to 40 μm, whereas the VoC-derived microvessels were significantly larger and more heterogeneous, ranging from 30 to 110 μm (Fig. 5B–iii).

To demonstrate the perfusability of the VUs-derived capillaries, fluorescent microbeads were injected into the VoC channel. As shown in Fig. 5C–i, in regions where VUs inosculated with the VoC channel, the flow was able to pass through the VoC into the VUs-derived capillaries, which also became perfused (Fig. 5C–ii), as evidenced by the presence of fluorescent microbeads flowing along them (Fig. 5C–iii).

Fig. 5D shows a robust VUs-derived microvessel network surrounding the VoC channel, along with 3D reconstruction images of selected regions (Fig. 5E i-iii) that clearly demonstrate the presence of fluorescent microbeads inside the lumen of VUs-derived capillaries. It also highlights the presence of the fibroblastic stromal network, surrounding both the VUs-derived capillaries and the VoC channel (Fig. 5E iv-vi). Collectively, these findings confirm the effective inosculation between the VUs and VoC channel, demonstrating the perfusability of the generated stromal-embedded microvascular 3D network.

3.5. VUs promote the formation of a vascularized stroma around IOs in the VoC

As a preliminary proof-of-concept, we assessed the potential of VUs to promote the formation of a vascularized stroma around intestinal organoids. Before co-culturing VUs with IOs in the VoC, we set out to replace Matrigel (MG), which is the standard 3D matrix for IOs culture, by fibrin-based hydrogels. We tested three different fibrin hydrogel formulations: Fib (non-supplemented fibrin, the one used for VUs culture); Fib-MG (fibrin supplemented with MG); and Fib-LEC (fibrin supplemented with LEC: laminin-entactin complex). The rheological characterization (Fig. 6A) demonstrated that Fib yielded a softer matrix compared to Matrigel (MG), while Fib-LEC hydrogels exhibited a significant increase in the G′ value, reaching levels comparable to MG. Despite the differences in rheological properties, the organoid formation efficiency (% of organoid development from single cysts) was similar between Fib-MG, Fib-LEC and MG (Fig. 6B). While Fib hydrogels alone did not support the growth of passaged IOs, the Fib-MG and Fib-LEC hydrogels facilitated the development of rounded cysts into characteristic crypt-like budding structures within 4 days. Over the course of 7 days, these structures underwent further maturation, displaying a

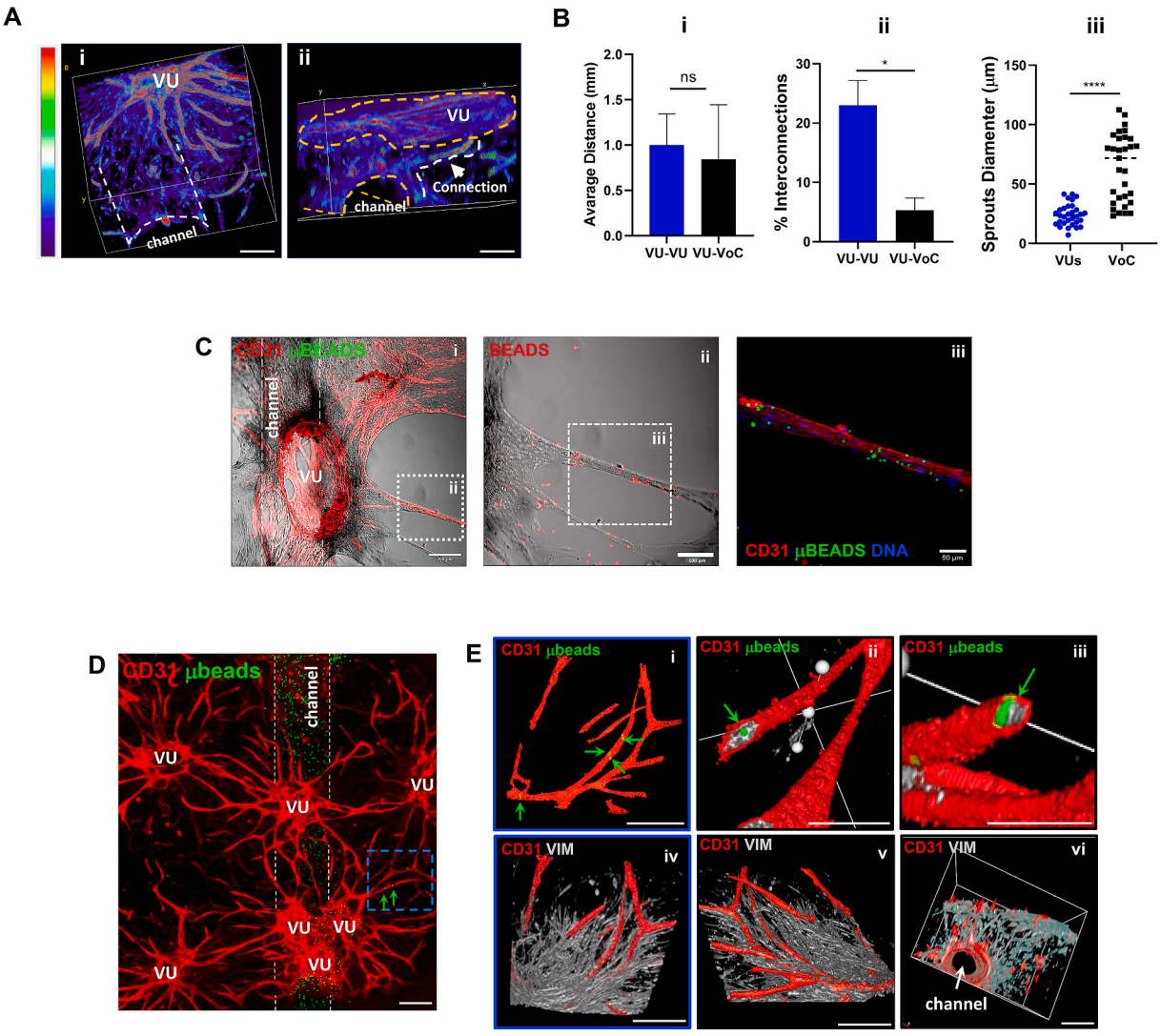

Fig. 5. Inosculation and perfusion of VUs-derived capillaries in the VoC. A) Representative Thermal Color LUT 3D reconstructions of UEA-I^{+} staining showing the (i) relative position and (ii) interconnection zones between VU and VoC (dark blue: low signal intensity, red: high signal intensity, scale bars: 200 μm). **B)** Quantification of: (i) average distance between VUs (VU-VU) and between VUs and the VoC (VU-VoC), (ii) percentage of VU-VU and VU-VoC interconnections, and (iii) average diameter of VUs-derived and channel-derived microvessels. In all graphs, statistically significant differences are marked with ** ($p < 0.01$) or *** ($p < 0.001$). (iv-v). **C)** Composite image of VUs connected with the VoC after 7 days of culture (red: CD31; green: fluorobeads, scale bar: 200 μm). (ii) High magnification image of the white dashed region (red: fluorobeads, scale bar: 100 μm. iii) high magnification image of white dashed region in ii (red: CD31, green: fluorobeads; blue: nuclei, scale bar: 50 μm. **D)** Confocal image showing VoC perfusion with fluorescent beads (2 μm) and perfusate infiltration into VUs-derived microvessels at day 7 (dashed lines: VoC; green arrows: infiltration of fluorescent beads inside VUs-derived microvessels; red: CD31, green: fluorescent beads; scale bar:200 μm. **E)** (i, iv and v) 3D reconstructions showing a higher magnification of Fig. 4D blue dashed zone and stromal network supporting VUs-derived microvessels (red: CD31, gray: vimentin, green: fluorescent beads; green arrows: fluorescent beads, scale bar: 200 μm). (ii and iii) 3D reconstruction from confocal z-stacks using clipping planes to reveal the presence of fluorescent beads located inside the lumen of VUs-derived microvessels (red: CD31, green: fluorescent beads; green arrows: fluorescent beads, scale bar: 200 μm). (vi) 3D representation of VoC showing a rich stromal compartment surrounding the vascular channel (red: CD31, gray: vimentin; scale bar: 200 μm).

growth pattern similar to that observed in MG (Fig. S9, Supporting information). As depicted in Fig. 6D, the IOs displayed budding structures surrounding the central lumen, similar to the intestinal crypt domain, with polarized cellular organization and expression of the epithelial marker β-catenin (Fig. 6C). Moreover, the budding domains were enriched in Ki67+ proliferative cells (Fig. 6D and i ii), and in terminally differentiated Paneth cells, as shown by the expression of *C*-type lysozyme (Fig. 6D iii, iv and Fig. S10, Supporting information).

We then tested the behavior of IOs when cultured in fibrin-based hydrogels in the VoC. Passaged organoids were embedded in Fib-MG or Fib-LEC hydrogel precursor solutions and added to the microfluidic device. After polymerization, the hollow channel was endothelized as previously described. Over time, in both hydrogels, IOs were able to grow and develop into more complex structures (Fig. 6E), interacting with the channel-derived endothelial sprouts close to the VoC channel walls.

Finally, to extend the microvascular network into the hydrogel bulk, passaged IOs were combined with VUs within the VoC (Fig. 6F). Both types of structures were dispersed in the fibrin hydrogels prior to polymerization, and 3 days later, the VUs already presented angiogenic sprouts, similar to those observed in non-supplemented Fib hydrogels, while the IOs continued to grow and differentiate (Fig. 6G). Over time, the VUs-derived capillaries progressively reached and enveloped the IOs (Fig. 6G and H), both proximal and distal to the VoC channel, expanding the microvascular network to multiple organoids. At the same time, the fibroblasts formed multicellular networks around the IOs, providing

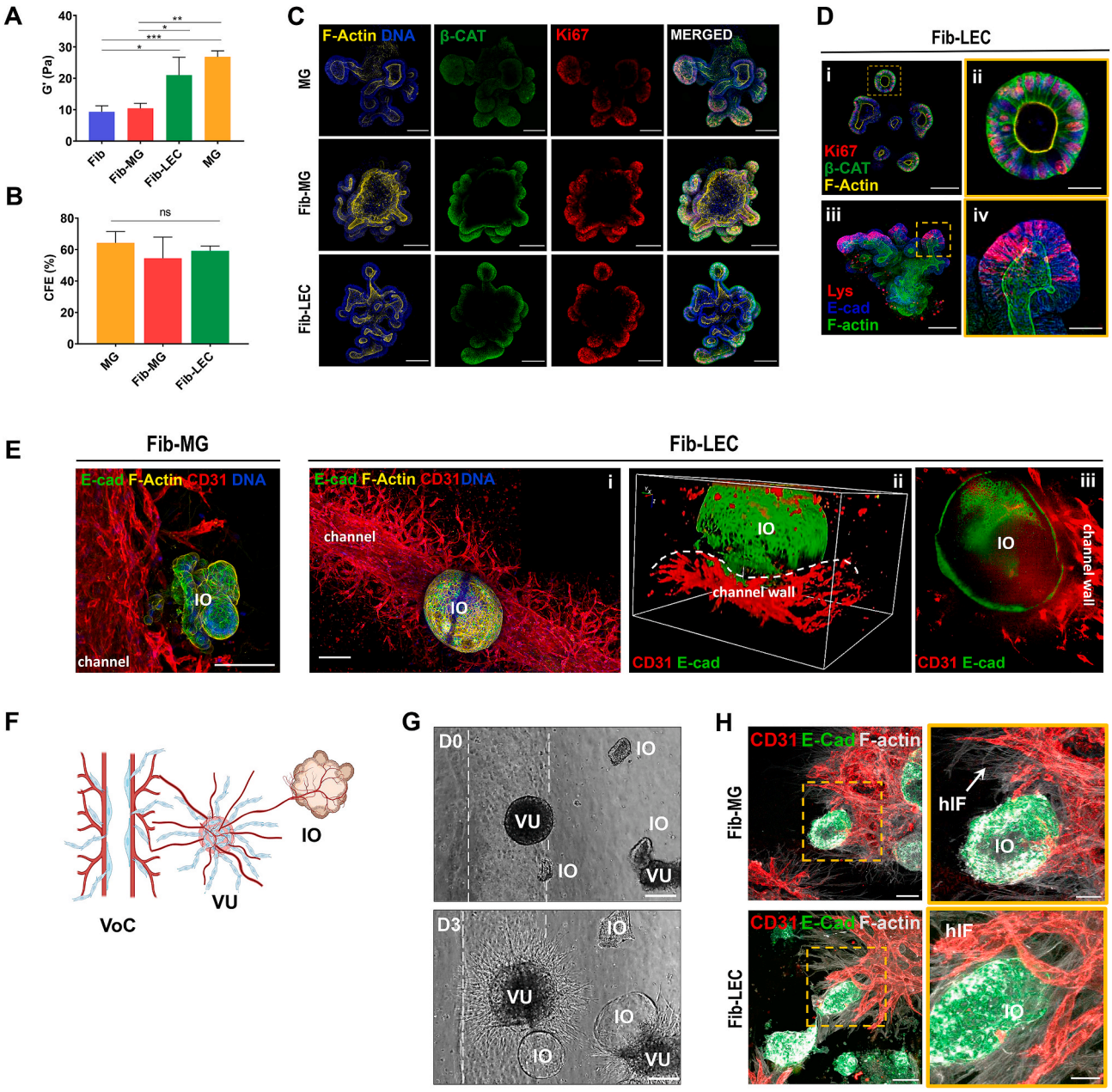

Fig. 6. VUs promote the formation of a vascularized stroma around IOs in the VoC. A) Single frequency sweep analysis of G′ of Fibrin, Fibrin-Matrigel, Fibrin-LEC and Matrigel (MG) during gelation (n = 3). **B)** Colony-forming efficiency of intestinal crypts embedded in different hydrogels. **C)** Representative immunofluorescence images of IOs cultured for 7 days in Fib-MG, Fib-LEC or MG showing similar morphology (yellow: F-actin, green: β-catenin, red: Ki67, blue: nuclei). Scale bars:100 μm. **D)** (i) Representative immunofluorescence images of IOs cultured in Fib-LEC showing proliferative Ki67+ cells (yellow: F-actin, green: β-catenin, red: KI67, blue: nuclei). Scale bar:100 μm. (ii) Higher magnification image of the yellow dashed region. Scale bar: 30 μm. (iii) Expression of the phenotypical intestinal marker lysozyme (green: F-actin, blue: *E*-cadherin, red: lysozyme). Scale bar:100 μm. (iv) Higher magnification image of the yellow dashed region. Scale bar: 30 μm. **E)** IOs embedded in Fib-MG or Fib-LEC hydrogels integrated into the microfluidic chamber and cultured in close contact with the VoC (yellow: F-actin, green: *E*-cadherin, red: CD31, blue: DNA). Scale bars: 100 μm. **F)** Graphical representation of the experimental approach where VUs promote IOs vascularization. Created with Biorender.com. **G)** Phase-contrast images of VUs and IO integrated into the microfluidic chamber and in close contact with the VoC at days 0 and 3. Scale bar: 100 μm. **H)** Fluorescent images depicting VUs-derived endothelial sprouts and rich stromal network in close proximity to IOs after 3 days of culture in Fib-MG or Fib-LEC (F-actin: gray, red: CD31, green: *E*-cadherin, blue: DNA). Scale bars: 100 μm (inset images: 50 μm).

additional stromal support to the system and enhancing its physiological relevance.

4. Discussion

The timely establishment of perfusable microvascular networks within engineered tissues and organs is essential to ensure their viability and function upon implantation. These microvascular networks should ideally develop *in situ*, adapting to the local microenvironment, and rapidly inosculate with host microvessels to extend blood flow throughout the entire 3D construct [4,33,34]. In this study, we present an innovative vascularization strategy based on the use of Vascular Units (VUs) as building blocks to generate stroma-embedded perfusable microvascular networks from the bottom-up. Thanks to their versatility and micro-sized nature, VUs can be directly injected into a lesion site or easily integrated into different types of 3D scaffolds before implantation.

In this study, we selected the small intestine as the target organ given the urgent need for tissue engineering solutions in intestinal wound healing, and the vital role of a supportive vascularized stroma in epithelial regeneration. Considering that fibroblasts from different tissues exhibit distinct molecular signatures, particularly in terms of ECM composition [35], we produced VUs combining ECFC with organ-specific intestinal fibroblasts to better mimic the vascularized stromal compartment of the small intestine. Several studies have emphasized the key role of stromal cells in the formation of vascularized microtissues, where they modulate EC behavior and assembly into lumenized capillary-like structures [8–10,14,36,37]. Stromal cells may also act as pericytes, contributing to the long-term stability of these structures [20,37–40]. Here, the presence of intestinal fibroblasts was central for ensuring the cohesiveness and structural integrity of the VUs, which could not be achieved when using ECFC alone (data not shown), as previously demonstrated with other stromal cell types [10]. Moreover, when VUs were embedded in fibrin, fibroblasts co-migrated into the hydrogel, secreting their own ECM. This contributed to the establishment of an optimal 3D microenvironment for vascular morphogenesis, resulting in the generation of robust capillary beds stabilized by interstitial matrix and a basement membrane layer, ultimately forming an ECM-rich vascularized stroma. We demonstrated that the VUs-derived capillaries presented well-defined lumens and were able to inosculate with capillaries from adjacent VUs, forming extensive microvessel 3D networks.

To further characterize the inosculation potential and perfusability of the VUs-derived capillaries, we designed a biomimetic fibrin-based vessel-on-chip (VoC). This microfluidic device imposed no geometrical restriction on vascular growth and supported the formation of hierarchical and interconnected microvessel networks, emulating the physiological behavior of native vasculature. It featured one or two fibrin-embedded hollow channels with diameter in the range of arterioles/venules, created using an acupuncture needle as the template. While not novel, this approach was very reproducible and more straightforward compared to sacrificial molding technique [14,41,42]. It was also versatile, as the channel diameter could be easily adjusted by selecting needles of different sizes. For endothelialization, it was necessary to coat the hollow channel with ECM proteins to facilitate cell attachment, and the co-seeding of hIF along with ECFC in the channel was essential to achieve a cohesive endothelial monolayer. Moreover, the density at which cells were seeded played a pivotal role in determining the angiogenic sprouting potential of the endothelialized channel. Higher cell densities promoted the formation of lumenized endothelial sprouts, and lower densities resulted in a steady endothelial layer, possibly due to insufficient coverage for a complete monolayer soon after seeding. While this has not been studied in detail herein, it is also possible that the effective adhesion ratio of hIF-to-ECFC to the channel varies under the different conditions, which in turn is likely to impact the behavior of ECFC. Moreover, prior research showed the positive impact of higher cell densities on angiogenic sprouting [43,44]. The open-ended endothelial sprouts that emerged from the VoC channel infiltrated the surrounding hydrogel, forming a vascular tree-like structure. They were also perfusable and non-leaky, as demonstrated by flow studies using fluorescent dextran (70 kDa) or fluorescent microbeads (2 μm). This dynamic feature of neo-vessel formation sets our model apart from other reported VoCs with steady vascular-like channels [45–47]. Of note, the fibrin-embedded hollow channels sustained different flow regimens without bursting, and the 2-channel set-up represents a step forward in modeling a closed circulation loop integrating both arteriole-like and venule-like flow [48]. While not further explored in this study, these are relevant features of the system that will allow exploring cells' response to fluid dynamics in future studies [3,49]. This VoC design offers some advantages over traditional PDMS-based organ-on-chip (OoC) platforms, namely: i) it delivers a biomimetic vascularized 3D construct, i.e., with no additional plastic components apart from the PLA housing; ii) it allows for the culture and recovery of large sample volumes, and iii) it allows the extraction of the entire vascularized 3D construct from the PLA housing without compromising its structural integrity. Overall, this greatly eases handling, monitoring, and downstream analysis.

When VUs were added to the fibrin hydrogel between 2 mm spaced channels within the VoC, the VUs-derived capillaries bridged the channels and contributed to the establishment of a robust microvascular network throughout the entire device. Notably, these microvascular structures were embedded in a stromal microenvironment rich in ECM and fibroblasts, which together supported the growth and stability of the capillary bed. The progressive stabilization of these vascular structures translated into a decrease in the mRNA expression of endothelial activation, angiogenesis, and matrix remodeling markers. These processes are regulated by VEGF/Notch signaling pathways, and vessel differentiation, linked to Notch activation, is characterized by cell cycle arrest and downregulation of VEGF-regulated endothelial gene expression markers, as observed herein [31,32].

The VUs-derived capillaries also successfully inosculated with capillaries from other VUs (VU-VU) and with the VoC channel-derived capillaries (VU-VoC). As a result, when the VoC channel was perfused, some of the VUs-derived capillaries also become perfused, as shown by the presence of fluorescent beads (used as tracers) inside their lumens. While the VoC could be continuously perfused, characterizing the perfusability of the VUs-derived networks was challenging due to the non-standard flow properties of the fluorescent microbeads. Indeed, the effective infiltration of the inosculated capillaries by the flowing microbeads was a highly probabilistic event, leading to an underestimation of the system's perfusion capability. Additionally, the use of fluorescent dextran was not ideal, as the presence of the open-ended endothelial sprouts promoted its rapid diffusion throughout the hydrogel matrix, creating imaging artifacts. Despite these limitations, our results clearly demonstrate that VUs are effectively able to functionally inosculate with larger diameter vessels. While requiring *in vivo* validation, this suggests their capability to connect with host vessels upon implantation, become blood-perfused, and form functional microvascular networks *in situ*. Notably, the use of VUs as a (micro)vascularization strategy can be explored to engineer various types of tissues and organs, highlighting their broad applicability in the regenerative medicine field.

The potential of VUs to generate extensive stroma-embedded microvascular networks within a VoC device and 'bridge' perfusable channels also represents a novel and relevant concept in the field of microphysiological systems. Indeed, such an approach could facilitate the establishment of microfluidic loops in VoC models lacking effective connections between two or more vascular channels [50–52]. Another important advantage of VUs is that they also contain fibroblasts, which gradually migrate into the hydrogel compartment, creating an ECM-rich stroma "on-chip". This is crucial for more accurately mimicking the natural environment of tissues/organs and advancing the field of OoC [53].

As a preliminary proof-of-concept, we demonstrated the ability of VUs to promote the formation of a vascularized stroma around intestinal organoids within the VoC. Before combining VUs with IOs, we had to optimize fibrin-based hydrogels for organoid culture, as fibrin alone proved to be unsuitable for IOs development. Fibrin supplemented with Matrigel or laminin-111/entactin complex (LEC) yielded excellent results, while also supporting the angiogenic sprouting potential of the VUs, allowing the successful combination of the different structures in the VoC. This is in accordance with previous findings from other authors showing that IOs cultured in LEC-supplemented fibrin hydrogels present colony formation efficiency and differentiation potential comparable to that of pure MG [54]. Thus, the supplemented fibrin hydrogels, particularly the Fib-LEC, offer an interesting alternative to Matrigel, as they present a more defined and consistent composition that may enhance the reproducibility of IOs culture [55]. When IOs were added to the supplemented fibrin hydrogels in the VoC they continued to grow, and those located close to the wall of the endothelialized channel became

rapidly surrounded by channel-derived capillaries. Therefore, the inclusion of VUs alongside IOs enabled the simultaneous vascularization of multiple organoids within the VoC, even those located distant from the VoC channel, while also forming a fibroblast-derived stromal tissue around them. This VUs-based strategy has the potential to substantially increase the surface contact area of IOs with a vascularized stroma and enable the culture of multiple organoids per chip, in contrast to other VoC platforms that have compartmentalized channels and space constraints [37,39,51]. Our results are promising, but future studies should focus on analyzing IOs functionality in the presence and absence of a vascularized stroma under perfusion.

Overall, the small size and high angiogenic sprouting potential of VUs establish them as versatile tools for engineering perfusable microvascular networks in various contexts. They can be: i) integrated into in vitro models to enhance their biomimicry, including in VoC platforms as illustrated herein; ii) combined with a vehicle and used in an injectable form for minimally invasive therapeutic vascularization [9]; or iii) combined with scaffolds [10] or with bioinks for bioprinting to create large-scale pre-vascularized 3D constructs.

5. Conclusions

In summary, we developed and characterized specialized Vascular Units (VUs) consisting of endothelial progenitor cells and organ-specific intestinal fibroblasts. We demonstrated their potential to serve as building blocks for the formation of lumenized capillaries and subsequent establishment of microvascular 3D networks within a hydrogel matrix. Using a customized biomimetic VoC, we showed the ability of VUs-derived capillaries to inosculate with larger-diameter vessels and become perfused. Lastly, by integrating VUs with IOs in the VoC, we illustrated how VUs can act as "vascularization bridges," extending a microvascular network throughout the hydrogel bulk and supporting the formation of a vascularized stroma around multiple organoids within a single microfluidic device. The versatility of VUs as tools in vascularization strategies opens a wide array of possibilities in tissue engineering, ranging from regenerative medicine to advanced microphysiological in vitro systems.

Ethics approval and consent to participate

Human umbilical cord blood was obtained from healthy donors following a protocol approved by the Ethics Committee of CHUSJ (Centro Hospitalar Universitário de São João, Porto, Portugal).

Data availability statement

The data that support the findings of this study are available from the corresponding author upon reasonable request.

CRediT authorship contribution statement

I.D. Orge: Conceptualization, Validation, Writing – original draft, Writing – review & editing, Data curation, Formal analysis, Investigation, Methodology, Visualization. **H. Nogueira Pinto:** Investigation, Methodology, Writing – review & editing. **M.A. Silva:** Investigation, Methodology, Writing – review & editing. **S.J. Bidarra:** Investigation, Methodology, Writing – review & editing. **S.A. Ferreira:** Investigation, Methodology, Validation, Writing – review & editing. **I. Calejo:** Investigation, Methodology, Writing – review & editing. **R. Masereeuw:** Conceptualization, Funding acquisition, Investigation, Methodology, Supervision, Writing – review & editing. **S.M. Mihăilă:** Conceptualization, Funding acquisition, Investigation, Methodology, Resources, Supervision, Writing – review & editing. **C.C. Barrias:** Conceptualization, Funding acquisition, Investigation, Methodology, Project administration, Resources, Supervision, Validation, Writing – original draft, Writing – review & editing.

Declaration of competing interest

The authors declare that they have no known competing financial interests or personal relationships that could have appeared to influence the work reported in this paper.

Acknowledgments

The work was developed under the scope of the EndoSWITCH project (PTDC/BTMORG/5154/2020), supported by the Portuguese Foundation for Science and Technology (FCT). The authors thanks FCT for Iasmim Orge's PhD scholarship SFRH/BD/2020.07458, Sílvia Bidarra's research contract DL 57/2016/CP1360/CT0006 and Silvia Ferreira's research contract CEECINST/00132/2021/CP1774/CT0001. Iasmim Orge thanks the training provided under the scope of the REMODEL project (European Union's Horizon 2020 research and innovation programme, grant agreement 7857491). The authors also acknowledge the support of i3S Scientific Platforms: "Bioimaging" member of the PPBI (Grant No: PPBI-POCI-01-0145-FEDER-022122), "Biointerfaces and Nanotechnology" (Grant No: UID/BIM/04293/2019) and "BioSciences Screening" (member of the PT-OPENSCREEN (NORTE-01-0145-FEDER-085468) and PPBI (PPBI-POCI-01-0145-FEDER-022122)).

Appendix A. Supplementary data

Supplementary data to this article can be found online at https://doi.org/10.1016/j.bioactmat.2024.05.021.

References

[1] H.G. Augustin, G.Y. Koh, Organotypic vasculature: from descriptive heterogeneity to functional pathophysiology, Science 357 (6353) (2017).
[2] B. Palikuqi, D.T. Nguyen, G. Li, R. Schreiner, A.F. Pellegata, Y. Liu, D. Redmond, F. Geng, Y. Lin, J.M. Gomez-Salinero, M. Yokoyama, P. Zumbo, T. Zhang, B. Kunar, M. Witherspoon, T. Han, A.M. Tedeschi, F. Scottoni, S.M. Lipkin, L. Dow, O. Elemento, J.Z. Xiang, K. Shido, J.R. Spence, Q.J. Zhou, R.E. Schwartz, P. De Coppi, S.Y. Rabbany, S. Rafii, Adaptable haemodynamic endothelial cells for organogenesis and tumorigenesis, Nature 585 (7825) (2020) 426–432.
[3] C. O'Connor, E. Brady, Y. Zheng, E. Moore, K.R. Stevens, Engineering the multiscale complexity of vascular networks, Nat. Rev. Mater. 7 (9) (2022) 702–716.
[4] J. Rouwkema, A. Khademhosseini, Vascularization and angiogenesis in tissue engineering: beyond creating static networks, Trends Biotechnol. 34 (9) (2016) 733–745.
[5] D. Wang, S. Maharjan, X. Kuang, Z. Wang, L.S. Mille, M. Tao, P. Yu, X. Cao, L. Lian, L. Lv, J.J. He, G. Tang, H. Yuk, C.K. Ozaki, X. Zhao, Y.S. Zhang, Microfluidic bioprinting of tough hydrogel-based vascular conduits for functional blood vessels, Sci. Adv. 8 (43) (2022) eabq6900.
[6] Z. Kong, X. Wang, Bioprinting Technologies and bioinks for vascular model establishment, Int. J. Mol. Sci. 24 (1) (2023).
[7] A. Dellaquila, C. Le Bao, D. Letourneur, T. Simon-Yarza, In vitro strategies to vascularize 3D physiologically relevant models, Adv. Sci. 8 (19) (2021) e2100798.
[8] E. Bauman, T. Feijao, D.T.O. Carvalho, P.L. Granja, C.C. Barrias, Xeno-free pre-vascularized spheroids for therapeutic applications, Sci. Rep. 8 (1) (2018) 230.
[9] T. Feijao, M.I. Neves, A. Sousa, A.L. Torres, S.J. Bidarra, I.D. Orge, D.T.O. Carvalho, C.C. Barrias, Engineering injectable vascularized tissues from the bottom-up: dynamics of in-gel extra-spheroid dermal tissue assembly, Biomaterials 279 (2021) 121222.
[10] D.T.O. Carvalho, T. Feijão, M.I. Neves, R.M.P. da Silva, C.C. Barrias, Directed self-assembly of spheroids into modular vascular beds for engineering large tissue constructs, Biofabrication 13 (3) (2021).
[11] K.L. Sinagoga, J.M. Wells, Generating human intestinal tissues from pluripotent stem cells to study development and disease, EMBO J. 34 (9) (2015) 1149–1163.
[12] S. Yamaguchi, K. Kanetaka, Y. Maruya, M. Higashi, S. Kobayashi, K. Hashiguchi, F. Oohashi, Y. Sakai, K. Nakao, S. Eguchi, Highly feasible procedure for laparoscopic transplantation of cell sheets under pneumoperitoneum in porcine model, Surg. Endosc. 36 (6) (2022) 3911–3919.
[13] K. Banno, M.C. Yoder, Tissue regeneration using endothelial colony-forming cells: promising cells for vascular repair, Pediatr. Res. 83 (1–2) (2018) 283–290.
[14] E.A. Margolis, D.S. Cleveland, Y.P. Kong, J.A. Beamish, W.Y. Wang, B.M. Baker, A. J. Putnam, Stromal cell identity modulates vascular morphogenesis in a microvasculature-on-a-chip platform, Lab Chip 21 (6) (2021) 1150–1163.
[15] H.A. Strobel, S.M. Moss, J.B. Hoying, Methods for vascularization and perfusion of tissue organoids, Mamm. Genome 33 (3) (2022) 437–450.
[16] S. Grebenyuk, A. Ranga, Engineering organoid vascularization, Front. Bioeng. Biotechnol. 7 (2019) 39.

[17] R.N. Gomes, F. Manuel, D.S. Nascimento, The bright side of fibroblasts: molecular signature and regenerative cues in major organs, NPJ Regen Med 6 (1) (2021) 43.

[18] D.A. Ingram, L.E. Mead, H. Tanaka, V. Meade, A. Fenoglio, K. Mortell, K. Pollok, M. J. Ferkowicz, D. Gilley, M.C. Yoder, Identification of a novel hierarchy of endothelial progenitor cells using human peripheral and umbilical cord blood, Blood 104 (9) (2004) 2752–2760.

[19] P.A. Williams, R.S. Stilhano, V.P. To, L. Tran, K. Wong, E.A. Silva, Hypoxia augments outgrowth endothelial cell (OEC) sprouting and directed migration in response to sphingosine-1-phosphate (S1P), PLoS One 10 (4) (2015) e0123437.

[20] A.L. Torres, S.J. Bidarra, D.P. Vasconcelos, J.N. Barbosa, E.A. Silva, D. S. Nascimento, C.C. Barrias, Microvascular engineering: dynamic changes in microgel-entrapped vascular cells correlates with higher vasculogenic/angiogenic potential, Biomaterials 228 (2020) 119554.

[21] P.G.M. Jochems, J. van Bergenhenegouwen, A.M. van Genderen, S.T. Eis, L.J. F. Wilod Versprille, H.J. Wichers, P.V. Jeurink, J. Garssen, R. Masereeuw, Development and validation of bioengineered intestinal tubules for translational research aimed at safety and efficacy testing of drugs and nutrients, Toxicol. Vitro 60 (2019) 1–11.

[22] C. Chen, P.G.M. Jochems, L. Salz, K. Schneeberger, L.C. Penning, S.F.J. van de Graaf, U. Beuers, H. Clevers, N. Geijsen, R. Masereeuw, B. Spee, Bioengineered bile ducts recapitulate key cholangiocyte functions, Biofabrication 10 (3) (2018) 034103.

[23] J. Jansen, I.E. De Napoli, M. Fedecostante, C.M. Schophuizen, N.V. Chevtchik, M. J. Wilmer, A.H. van Asbeck, H.J. Croes, J.C. Pertijs, J.F. Wetzels, L.B. Hilbrands, L. P. van den Heuvel, J.G. Hoenderop, D. Stamatialis, R. Masereeuw, Human proximal tubule epithelial cells cultured on hollow fibers: living membranes that actively transport organic cations, Sci. Rep. 5 (2015) 16702.

[24] E. Filova, E. Brynda, T. Riedel, J. Chlupac, M. Vandrovcova, Z. Svindrych, V. Lisa, M. Houska, J. Pirk, L. Bacakova, Improved adhesion and differentiation of endothelial cells on surface-attached fibrin structures containing extracellular matrix proteins, J. Biomed. Mater. Res. 102 (3) (2014) 698–712.

[25] T. Sato, R.G. Vries, H.J. Snippert, M. van de Wetering, N. Barker, D.E. Stange, J. H. van Es, A. Abo, P. Kujala, P.J. Peters, H. Clevers, Single Lgr5 stem cells build crypt-villus structures in vitro without a mesenchymal niche, Nature 459 (7244) (2009) 262–265.

[26] A.D. Gracz, B.J. Puthoff, S.T. Magness, Identification, isolation, and culture of intestinal epithelial stem cells from murine intestine, Methods Mol. Biol. 879 (2012) 89–107.

[27] D.P. Ivanov, T.L. Parker, D.A. Walker, C. Alexander, M.B. Ashford, P.R. Gellert, M. C. Garnett, Multiplexing spheroid volume, resazurin and acid phosphatase viability assays for high-throughput screening of tumour spheroids and stem cell neurospheres, PLoS One 9 (8) (2014) e103817.

[28] R. Haase, L.A. Royer, P. Steinbach, D. Schmidt, A. Dibrov, U. Schmidt, M. Weigert, N. Maghelli, P. Tomancak, F. Jug, E.W. Myers, CLIJ: GPU-accelerated image processing for everyone, Nat. Methods 17 (1) (2020) 5–6.

[29] J. Eglinger, H. Karsjens, E. Lammert, Quantitative assessment of angiogenesis and pericyte coverage in human cell-derived vascular sprouts, Inflamm. Regen. 37 (2017) 2.

[30] G. Carpentier, S. Berndt, S. Ferratge, W. Rasband, M. Cuendet, G. Uzan, P. Albanese, Angiogenesis analyzer for ImageJ - a comparative morphometric analysis of "endothelial tube formation Assay" and "fibrin bead Assay", Sci. Rep. 10 (1) (2020) 11568.

[31] E. Trimm, K. Red-Horse, Vascular endothelial cell development and diversity, Nat. Rev. Cardiol. 20 (3) (2023) 197–210.

[32] N.W. Chavkin, G. Genet, M. Poulet, E.D. Jeffery, C. Marziano, N. Genet, H. Vasavada, E.A. Nelson, B.R. Acharya, A. Kour, J. Aragon, S.P. McDonnell, M. Huba, G.M. Sheynkman, K. Walsh, K.K. Hirschi, Endothelial cell cycle state determines propensity for arterial-venous fate, Nat. Commun. 13 (1) (2022) 5891.

[33] S. Fleischer, D.N. Tavakol, G. Vunjak-Novakovic, From arteries to capillaries: approaches to engineering human vasculature, Adv. Funct. Mater. 30 (37) (2020).

[34] M.A. Traore, S.C. George, Tissue engineering the vascular tree, Tissue Eng., Part B 23 (6) (2017) 505–514.

[35] L. Muhl, G. Genove, S. Leptidis, J. Liu, L. He, G. Mocci, Y. Sun, S. Gustafsson, B. Buyandelger, I.V. Chivukula, A. Segerstolpe, E. Raschperger, E.M. Hansson, J.L. M. Bjorkegren, X.R. Peng, M. Vanlandewijck, U. Lendahl, C. Betsholtz, Single-cell analysis uncovers fibroblast heterogeneity and criteria for fibroblast and mural cell identification and discrimination, Nat. Commun. 11 (1) (2020) 3953.

[36] N. Walji, S. Kheiri, E.W.K. Young, Angiogenic sprouting dynamics mediated by endothelial-fibroblast interactions in microfluidic systems, Adv Biol (Weinh) 5 (11) (2021) e2101080.

[37] M. Vila Cuenca, A. Cochrane, F.E. van den Hil, A.A.F. de Vries, S.A.J. Lesnik Oberstein, C.L. Mummery, V.V. Orlova, Engineered 3D vessel-on-chip using hiPSC-derived endothelial- and vascular smooth muscle cells, Stem Cell Rep. 16 (9) (2021) 2159–2168.

[38] I. Orellano, A. Thomas, A. Herrera, E. Brauer, D. Wulsten, A. Petersen, L. Kloke, G. N. Duda, Engineering vascular self-assembly by controlled 3D-printed cell placement, Adv. Funct. Mater. 32 (52) (2022) 2208325.

[39] U. Arslan, M. Brescia, V. Meraviglia, D.M. Nahon, R.W.J. van Helden, J.M. Stein, F. E. van den Hil, B.J. van Meer, M. Vila Cuenca, C.L. Mummery, V.V. Orlova, Vascularized hiPSC-derived 3D cardiac microtissue on chip, Stem Cell Rep. 18 (7) (2023) 1394–1404.

[40] A.L. Torres, S.J. Bidarra, M.T. Pinto, P.C. Aguiar, E.A. Silva, C.C. Barrias, Guiding morphogenesis in cell-instructive microgels for therapeutic angiogenesis, Biomaterials 154 (2018) 34–47.

[41] S. Salameh, N. Tissot, K. Cache, J. Lima, I. Suzuki, P.A. Marinho, M. Rielland, J. Soeur, S. Takeuchi, S. Germain, L. Breton, A perfusable vascularized full-thickness skin model for potential topical and systemic applications, Biofabrication 13 (3) (2021).

[42] T. Sano, T. Nakajima, K.A. Senda, S. Nakano, M. Yamato, Y. Ikeda, H. Zeng, J. I. Kawabe, Y.T. Matsunaga, Image-based crosstalk analysis of cell-cell interactions during sprouting angiogenesis using blood-vessel-on-a-chip, Stem Cell Res. Ther. 13 (1) (2022) 532.

[43] J.A. Whisler, M.B. Chen, R.D. Kamm, Control of perfusable microvascular network morphology using a multiculture microfluidic system, Tissue Eng. C Methods 20 (7) (2014) 543–552.

[44] B.M. Huuskes, R.J. DeBuque, P.G. Kerr, C.S. Samuel, S.D. Ricardo, The use of live cell imaging and automated image analysis to assist with determining optimal parameters for angiogenic Assay in vitro, Front. Cell Dev. Biol. 7 (2019) 45.

[45] M.N.S. de Graaf, A. Vivas, D.G. Kasi, F.E. van den Hil, A. van den Berg, A.D. van der Meer, C.L. Mummery, V.V. Orlova, Multiplexed fluidic circuit board for controlled perfusion of 3D blood vessels-on-a-chip, Lab Chip 23 (1) (2022) 168–181.

[46] Y. Wu, Y. Zhou, R. Paul, X. Qin, K. Islam, Y. Liu, Adaptable microfluidic vessel-on-a-chip platform for investigating tumor metastatic transport in bloodstream, Anal. Chem. 94 (35) (2022) 12159–12166.

[47] Vo, Q.; Carlson, K. A.; Chiknas, P. M.; Brocker, C. N.; DaSilva, L.; Clark, E.; Park, S. K.; Ajiboye, A. S.; Wier, E. M.; Benam, K. H., On-chip reconstitution of uniformly shear-sensing 3D matrix-embedded multicellular blood microvessel. Adv. Funct. Mater. n/a (n/a), 2304630..

[48] A.R. Murphy, M.C. Allenby, In vitro microvascular engineering approaches and strategies for interstitial tissue integration, Acta Biomater. 171 (2023) 114–130.

[49] S. Liu, Z. Lin, Vascular smooth muscle cells mechanosensitive regulators and vascular remodeling, J. Vasc. Res. 59 (2) (2022) 90–113.

[50] D. Ferrari, A. Sengupta, L. Heo, L. Pethö, J. Michler, T. Geiser, V.A. de Jesus Perez, W.M. Kuebler, S. Zeinali, O.T. Guenat, Effects of biomechanical and biochemical stimuli on angio- and vasculogenesis in a complex microvasculature-on-chip, iScience 26 (3) (2023) 106198.

[51] F. Bonanini, D. Kurek, S. Previdi, A. Nicolas, D. Hendriks, S. de Ruiter, M. Meyer, M. Clapés Cabrer, R. Dinkelberg, S.B. García, B. Kramer, T. Olivier, H. Hu, C. López-Iglesias, F. Schavemaker, E. Walinga, D. Dutta, K. Queiroz, K. Domansky, B. Ronden, J. Joore, H.L. Lanz, P.J. Peters, S.J. Trietsch, H. Clevers, P. Vulto, In vitro grafting of hepatic spheroids and organoids on a microfluidic vascular bed, Angiogenesis 25 (4) (2022) 455–470.

[52] Y. Nashimoto, T. Hayashi, I. Kunita, A. Nakamasu, Y.S. Torisawa, M. Nakayama, H. Takigawa-Imamura, H. Kotera, K. Nishiyama, T. Miura, R. Yokokawa, Integrating perfusable vascular networks with a three-dimensional tissue in a microfluidic device, Integr. Biol. 9 (6) (2017) 506–518.

[53] C.M. Leung, P. de Haan, K. Ronaldson-Bouchard, G.-A. Kim, J. Ko, H.S. Rho, Z. Chen, P. Habibovic, N.L. Jeon, S. Takayama, M.L. Shuler, G. Vunjak-Novakovic, O. Frey, E. Verpoorte, Y.-C. Toh, A guide to the organ-on-a-chip, Nature Reviews Methods Primers 2 (1) (2022) 33.

[54] N. Broguiere, L. Isenmann, C. Hirt, T. Ringel, S. Placzek, E. Cavalli, F. Ringnalda, L. Villiger, R. Zullig, R. Lehmann, G. Rogler, M.H. Heim, J. Schuler, M. Zenobi-Wong, G. Schwank, Growth of epithelial organoids in a defined hydrogel, Adv. Mater. 30 (43) (2018) e1801621.

[55] V. Magno, A. Meinhardt, C. Werner, Polymer hydrogels to guide organotypic and organoid cultures, Adv. Funct. Mater. 30 (48) (2020) 2000097.